electronic reprint

JOURNAL OF SYNCHROTRON RADIATION

ISSN: 1600-5775
journals.iucr.org/s

Wavefront-propagation simulations supporting the design of a time-delay compensating monochromator beamline at FLASH2

Mabel Ruiz-Lopez, Liubov Samoylova, Günter Brenner, Masoud Mehrjoo, Bart Faatz, Marion Kuhlmann, Luca Poletto and Elke Plönjes

J. Synchrotron Rad. (2019). **26**, 899–905

JOURNAL OF SYNCHROTRON RADIATION
ISSN 1600-5775

Wavefront-propagation simulations supporting the design of a time-delay compensating monochromator beamline at FLASH2[1]

Mabel Ruiz-Lopez,[a]* Liubov Samoylova,[b] Günter Brenner,[a] Masoud Mehrjoo,[a] Bart Faatz,[a] Marion Kuhlmann,[a] Luca Poletto[c] and Elke Plönjes[a]

[a]DESY, 22607 Hamburg, Germany, [b]European XFEL, 22869 Schenefeld, Germany, and [c]National Research Council Institute of Photonics and Nanotechnologies, 35136 Padova, Italy. *Correspondence e-mail: mabel.ruiz-lopez@desy.de

Received 26 October 2018
Accepted 11 March 2019

Edited by P. Fuoss, SLAC National Accelerator Laboratory, USA

[1] This article will form part of a virtual special issue on X-ray free-electron lasers.

Keywords: wavefront propagation; monochromators; diffraction gratings; ultrafast optics; wavefront simulations; free-electron lasers.

Wavefront-propagation simulations have been performed to complete the design of a monochromator beamline for FLASH2, the variable-gap undulator line at the soft X-ray free-electron laser in Hamburg (FLASH). Prior to propagation through the beamline optical elements, the parameters of the photon source were generated using the *GENESIS* code which includes the free-electron laser experimental data. Threshold tolerances for the misalignment of mirror angles are calculated and, since diffraction effects were included in the simulations, the minimum quality with respect to the slope errors required for the optics is determined.

1. Introduction

FLASH, the soft X-ray free-electron laser in Hamburg, has extraordinary properties: high brilliance [10^{28}–10^{31} photons s^{-1} mm^{-2} $mrad^{-2}$ (0.1% bandwidth)$^{-1}$] and ultrashort pulse duration (10–200 fs) in combination with a high repetition rate of up to 8000 pulses s^{-1} in burst mode (Ackermann *et al.*, 2007; Faatz *et al.*, 2016). However, the SASE (self-amplified spontaneous emission) spectrum contains an inherent bandwidth on the order of typically 0.5–1% (Tanikawa *et al.*, 2016), and the average wavelength as well as other beam parameters fluctuate from pulse to pulse because of the stochastic nature of the SASE process. Monochromator beamlines that are based on a single diffraction grating are used to reduce the free-electron laser (FEL) bandwidth for high-resolution spectroscopy experiments (Martins *et al.*, 2006; Gerasimova *et al.*, 2011); however they come at a price. Because of the pulse front tilt introduced by the grating a temporal stretching of the photon pulse occurs, thus increasing the photon-pulse duration. The installation of a time-delay compensating monochromator (TDCM) that preserves the pulse length (beamline FL23) will bring new scientific opportunities for experiments requiring both a narrower bandwidth and ultrashort pulses, such as solid-state and surface physics.

The key task is to design the beamline such that it transports the soft X-ray radiation to the user experiment while preserving the FEL beam quality, *i.e.* high photon energy and ultrashort pulses. The present work aims to model and optimize the design concept described by Poletto *et al.* (2018). By using wavefront simulations instead of ray tracing, further insights into the mechanical stability are provided and the optical quality required for each element can be defined. This is necessary to prevent obstacles during the construction, installation and operation of the monochromator beamline.

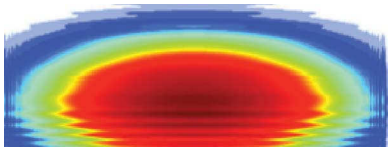

For many decades, ray-tracing codes have been used for the optical design of synchrotron beamlines, such as the *ShadowOui* code (Rebuffi & Sánchez del Río, 2016; Sanchez del Rio *et al.*, 2016). Although codes based on geometrical optics work well for non-coherent radiation, they do not characterize the diffraction effects of coherent sources, like FELs. For these sources, scalar wavefront-propagation theory is a better approach since it considers coherence properties.

Wavefront-propagation simulations for large facilities are supported by various codes (*i.e. PHASE*) or frameworks based on *SRW* (*Synchrotron Radiation Workshop*) like *Sirepo* (Rakitin *et al.*, 2017) or the *WavePropaGator* (*WPG*) package (Samoylova *et al.*, 2016). The latter was developed at the European XFEL for scientists involved in the optical design of FELs. It is an open source, user-friendly and very suitable tool to enhance the design of a new beamline. One important advantage of the *WPG* framework is that the definition of the implemented optical elements, *e.g.* elliptical mirrors, allows intuitive specification of the rotation angles. For other *SRW* frameworks, the coordinate system is based on the nominal output optical axis and the normal and tangential surface vectors. Considering this, we have upgraded *WPG* by including misalignments of the optics, *i.e.* yaw (γ), roll (ρ) and pitch (ζ) angles. As will be shown in the following, this new version provides simulations of the beam with better accuracy making the code a robust tool for determining the behavior of beam propagation in various beamline scenarios.

The paper is structured as follows. In the next section, the optical design of the TDCM beamline and the description of the source parameters are presented. In Section 3, we describe the upgraded version of the *WPG* package. Lastly, in Section 4, the results of the simulations, including the effects of mirror surface roughness and optics misalignment on the beamline focus are discussed. Furthermore, footprint sizes of the beam at the first grating are also given.

2. Time-delay compensating monochromator

2.1. Optical design

For many research areas that require a narrower bandwidth of the photon pulse than the natural bandwidth of FLASH, ultrashort pulse lengths (<50 fs) and a high peak brightness are still prerequisites. An ultrashort pulse length can be preserved using a two-grating monochromator design (Poletto *et al.*, 2018). To maximize the beamline throughput and transmission efficiency, the number of optical elements is minimized in the TDCM beamline. The TDCM utilizes six optical elements: a planar elliptical mirror (EM), two variable-line-spacing gratings in reflection mode (G1 and G2), a slit (S), a planar mirror (PM) and a bendable Kirkpatrick–Baez (KB) focusing system as shown in the sketch of the beamline in Fig. 1. The FEL radiation impinges at 2.5° grazing incidence on the EM with a central radius of curvature of 528 m, placed 68.9 m away from the last undulators. The EM deflects the FEL beam horizontally into the new beamline FL23, illuminating the first grating and focusing the horizontally dispersed radiation onto the exit slit of the first monochromator stage. The EM has a demagnification factor of 5.7. Two sets of gratings are envisaged within this monochromator stage: one covers the range for short wavelengths (λ = 1.2–6 nm) and one for longer wavelengths (λ = 6–20 nm). The former has a central groove density of 600 mm^{-1} and the latter one has a groove density of 150 mm^{-1}. Space for a third grating set is provided for future upgrades. A second set of gratings (with the same parameters) is installed behind the slit in the second monochromator stage, however with an important difference: the second grating is working in inside order configuration, whereas for the first grating the outside order is selected. In this way the optical path difference (OPD) introduced by the grating dispersion – and thus the pulse front tilt – can be compensated for all wavelengths. The OPD can be calculated according to Poletto *et al.* (2009) as $Nm\lambda$, where N is the number of grooves illuminated, m is the grating diffraction order and λ is the wavelength.

An additional advantage of this design is that the focus size of the KB optics is dependent only on the FEL source parameters, while the slit width can be varied with respect to the desired resolution and throughput without affecting the focal spot dimensions since the monochromator image at the exit slit is small compared with the slit width.

Upstream of G2, the PM brings the radiation upwards by 4° to compensate the vertical angle introduced by the KB optics. Thus, a horizontal photon beam is provided to the user experiments. The PM is positioned before the second grating keeping the beamline short enough to fit into the experimental

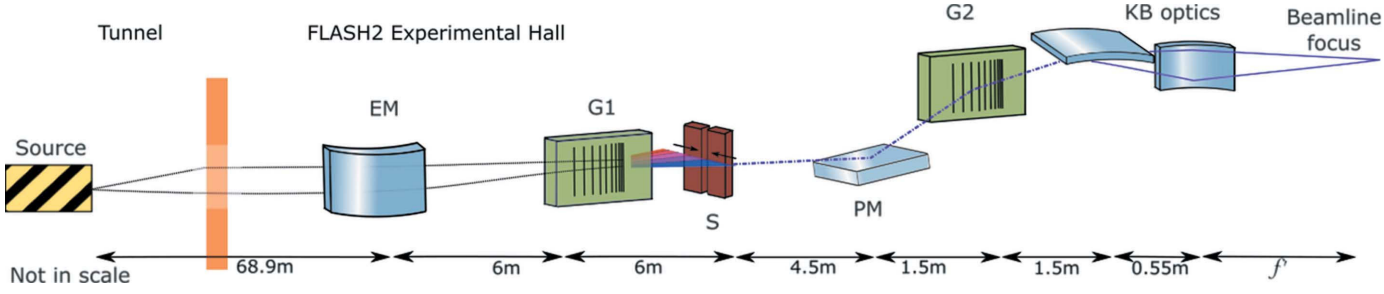

Figure 1
Time-delay compensating monochromator optical layout, made up of an elliptical mirror (EM), two gratings in compensating order (G1 and G2), a slit (S), a planar mirror (PM) and a variable KB optical system. The typical KB focal length is 2 m.

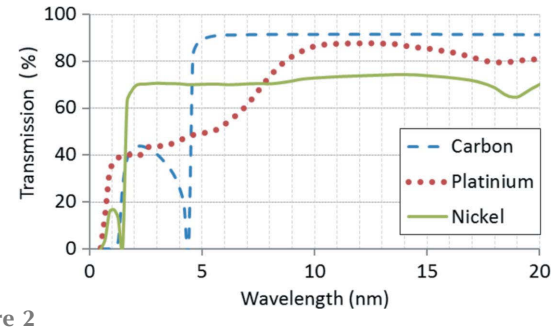

Figure 2
Total transmission of the two KB mirrors at 2° incident angle for platinum, nickel and carbon.

hall. Finally, the photon beam is focused using KB optics developed by FERMI@Elettra (Raimondi *et al.*, 2014). The focusing system includes bendable mirrors equipped with three different coatings optimized to provide the highest transmission over the entire wavelength range: platinum (for the shortest wavelengths), nickel (wavelength range between 3.6 and 6 nm) and carbon (for the longer wavelengths). Planned upgrades of FLASH will permit working with the second and third harmonics of the shortest generated wavelength, ∼3.6 nm, obtaining usable wavelengths in the 1.2–2.4 nm range. Fig. 2 shows the expected total transmission of the beamline after the KB optics. Vertically, the photon-source size is imaged by the KB optics onto the beamline focus with a demagnification of 35 assuming a source position at the end of the FLASH2 undulator section. The horizontal demagnification, given by a factor of ∼23, is however obtained by the product of the demagnification of the EM and the ratio of the distances from the slit to the first KB mirror and the focus distance given by the first KB mirror. The total length of the TDCM beamline including all elements (start-to-end) is 20.05 m. A first design was presented by Poletto *et al.* (2018) and by Frassetto *et al.* (2014).

The user requirements are summarized in Table 1.

Table 1
User requirements for the time-delay compensating monochromator for FLASH2.

Parameter	Value
Wavelength (nm)	1.2–20.0†
Pulse length (fs)	20–50–100
Resolution ($\lambda/\Delta\lambda$)	>2000
Peak brightness at the end of the beamline (photons pulse^{-1})	10^{10}

† Including the high harmonics.

2.2. Properties of the FLASH2 photon source

A consistent wavefront simulation requires precise characterization of the source. We have selected two features that are especially important for the design of the TDCM beamline: (i) the FEL spectrum and (ii) the beam divergence. With respect to the spectrum, even for the relatively narrow bandwidth of the FEL source, a monochromator is required to further reduce the bandwidth of the fundamental and/or filter out higher harmonics or, alternatively, the fundamental. Full attenuation of harmonics or undesired parts of the spectrum is difficult using solid filters or a gas-filled attenuator (Tiedtke *et al.*, 2013). For high-resolution spectroscopy, a resolving power on the order of $\lambda/\Delta\lambda \simeq 2000$–$3000$ is typically sufficient. According to the FEL parameters obtained during various experiments in 2018, the code *GENESIS* 1.3 (Reiche, 1999) was used to calculate the divergence, $\sigma_{\rm div}$, in µrad and the FEL spectrum. Fig. 3(*a*) shows a calculation of the FLASH2 spectrum for λ = 13 nm with a bandwidth of ∼0.5%. Fig. 3(*b*) shows the divergence for different wavelengths. The divergence obeys the following curve: $\sigma_{\rm div(FWHM)} = -0.59\lambda^2 + 23\lambda - 80$, for wavelengths between 8 nm and 20 nm. Assuming that diffraction-limited radiation produces a Gaussian beam, the corresponding photon-source size values are calculated using $\phi_{\rm FWHM} = (2\lambda)/(\pi\sigma) \simeq 70$–$80$ µm (Huang *et al.*, 2013).

3. *WPG* framework

The *WPG* framework was developed at the European XFEL for beamline scientists at FELs (Samoylova *et al.*, 2016). The wavefront propagation is performed using the Huygens–Fresnel principle along the z direction, in a space defined by x and y coordinates. The Fourier optics approach is used to describe the interaction of the radiation with each individual optical element. The code provides information about intensity and phase, and includes the definition of optics used, *e.g.* elliptical, planar and spherical mirrors, gratings, *etc*. Gratings were simulated in zeroth order to speed up our calculations since the phase shift is not taken into account for the results

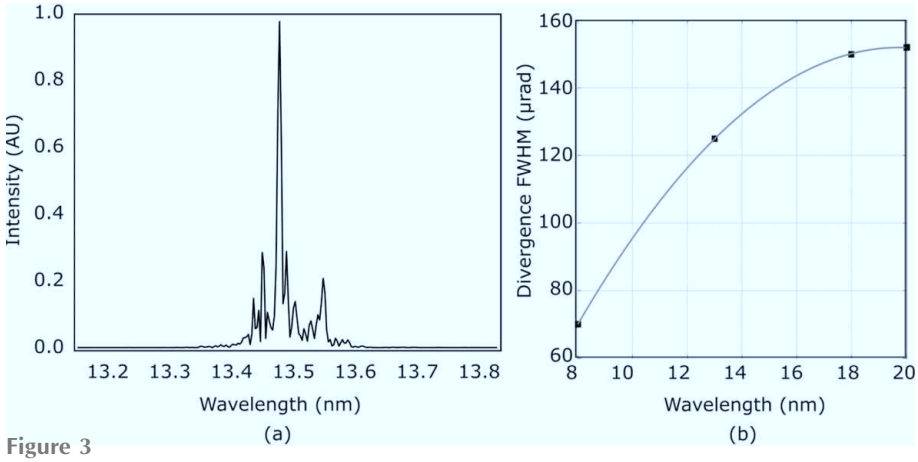

Figure 3
(*a*) Wavelength spectrum and (*b*) divergence, both calculated with *GENESIS* for FLASH2 parameters: an energy of 1.04 GeV, an emittance of 1.4 mm mrad, a current of 2.5 kA, an electron-bunch length of 10 µm and 7 undulators without tapering.

shown here. Measured data can be included to further characterize the optics, *e.g.* residual surface errors. The interactive framework package interfaces with Python scripts, offering the possibility of adapting the structure to each specific case. In the original version, *WPG* assumes a perfect alignment of the optics in the incident angle θ. We have implemented an upgrade in the code, allowing simulations containing misalignments in the optic positions with respect to the photon beam, *i.e.* in γ, ρ and ζ rotation angles. The upgraded version is a modification of the objects (functions) that describe reflecting surfaces, *i.e.* planar or elliptical mirrors. A new coordinate system is defined, where the direction of propagation z is specified for new x and y coordinates. The normal direction of optics is defined in coordinates n_x, n_y and n_z, perpendicular to the optical surface defined by t_x and t_y.

The new direction of propagation z' caused by misalignment can be expressed with the following coordinates for a mirror oriented vertically,

$$z' = \begin{bmatrix} n_x = \cos(\theta) & n_y = \sin(\rho) & n_z = -\sin(\theta) \\ t_x = -\sin(\theta) & t_y = 0 & t_z = 0 \\ x = \tan(\gamma)d & y = 0 & z \end{bmatrix}, \quad (1)$$

where d is the distance to the next optical element.

4. Results: wavefront simulation

Wavefront propagation through different optical elements is highly relevant for understanding the radiation behavior at FELs, where the radiation is spatially coherent. Ray-tracing calculations are not adequately precise in this case since they are limited to transversally incoherent beams. To optimize the design of the monochromator beamline, simulations need to account for diffraction effects. The design shall evaluate alignment tolerances, the footprint of the beam on the optics and deviations from the ideal optical surface (figure error) caused by the fabrication process. Overall, the versatility of the *WPG* framework for optimizing the TDCM beamline was very beneficial since the code includes important implementations: (i) the possibility to propagate the coherent FEL beam across mirrors with measured or simulated aberrated figure errors, (ii) it provides accurate footprints taking into account diffraction effects and (iii) the new upgraded version presented here supports movements in all axes and thus allows investigations of tolerances in the mirror alignment. In the following, the results of the studies with respect to the beam-footprint size at the first grating G1 as an example, effects of misalignment of the EM and the influence of mirror figure errors are presented.

4.1. Beam size in terms of the footprint

Manufacturing costs for a given optics can vary significantly depending on its physical dimensions. Thus, the calculation of the beam footprint on the optics is mandatory to determine the required length of the mirrors and gratings to maximize the beamline transmission. By calculating the FWHM of the beam on the surface of the optics, one obtains numbers that can be used to make a compromise between photon-energy losses, caused by clipping, and optical length available. For the FLASH2 monochromator beamline, the *WPG* simulations showed that the gratings are the elements in the beamline limiting the throughput most (see Table 2), therefore it was required to calculate the footprints at their position. To calculate these footprints, the values of divergence shown in Fig. 3(*b*) are used, *i.e.* $\theta_{\rm div}$ = 125 mrad at λ = 13 nm.

Table 2
Beam size and footprint in FWHM at the TDCM optics position.

	Beam horizontal (mm)	Beam vertical (mm)	Footprint horizontal (mm)	Footprint vertical (mm)
EM	8.2	8.4	187.0	8.4
G1	4.1	9.4	78.3	9.35
PM	3.1	10.6	3.1	303
G2	4.3	10.8	82.1	10.8
Vertical KB	5.3	11.0	5.3	316.0
Horizontal KB	4.3	8.8	123.0	8.81

For long wavelengths (*i.e.* 20 nm) the footprint obtained on the grating was FWHM = 110 mm (also read as $4\sigma \simeq 187$ mm). A 200 mm length grating is suggested in order to cover at least 4σ of the beam for larger wavelengths.

4.2. Effects of optics misalignments

WPG simulations show that misalignments of the EM with respect to ρ and ζ at the milliradian scale are negligible for the beam quality on the following grating G1 and the exit slit. However, rotations of the γ angle have a dramatic influence on the footprint shape and may produce, for instance, knife-edge diffraction effects if the beam encounters an optical edge. The γ angle misorientation has implications during the alignment of the beamline and it is important to quantify those effects. Based on these calculations, the precision on the mirror movements can be defined for the design process of the optical chambers. An experimental study in FLASH showed that γ angle misalignment require a precision in the micro-radian scale (Flöter *et al.*, 2010).

Fig. 4 compares the γ rotation effect for γ = 0.3 mrad using ray-tracing calculations performed with *ShadowOui* [Fig. 4(*a*)] and our *WPG* wavefront calculations [Fig. 4(*b*)]. While both figures show an asymmetry of the footprint, the *WPG* modeling shows the diffraction fringes at the edge of the mirror. Indeed, diffraction effects included in the wavefront calculations affect the quality of the central beam while ray-tracing calculations show instead a sharp edge that does not clip the central beam or has any other important impact on the beam properties. Adding slope error (RMS < 0.3 nm) to misaligned optics has almost no effect on the footprint profiles.

4.3. Influence of the mirror figure error on the focus quality

The mirror figure error is defined as the deviations of a mirror from an ideal optical surface. These deviations affect the wavefront quality of the beam and thus its propagation, causing an increase in the size of the focused beam. In order to classify the effects of the deviations versus the figure error, we

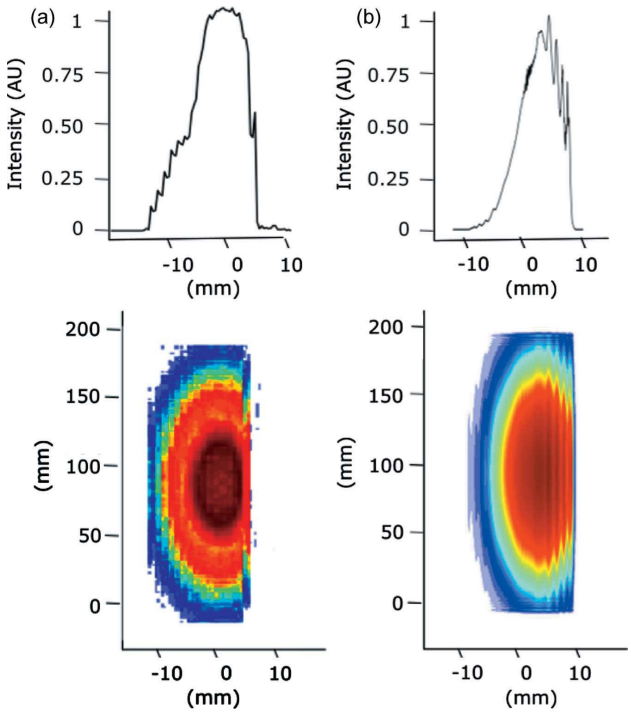

Figure 4
Calculation of the illumination distribution pattern on the grating G1 for an EM misaligned at the γ rotation by γ = 0.3 mrad. (*a*) Ray-tracing computation realized with *ShadowOui*. (*b*) Wavefront calculation realized with *WPG*.

determined the intensity distribution at the focus for three cases: (*a*) ideal optics, KB mirrors with a figure error σ_{RMS} = 0.0 nm; (*b*) σ_{RMS} < 0.3 nm, which is achieved for the optics in a similar system installed at FLASH beamline FL24; and (*c*) σ_{RMS} < 0.6 nm, for demonstration of the effect in the wavefront propagation.

Since the calculations have been made prior to the fabrication of the mirror, we instead used a modified figure error of a similar focusing system installed in the beamline FL24. The optical system includes the figure error for two alignment mirrors in the tunnel of the FEL and the figure error for the PM downstream of the second grating G2. The accuracy of *WPG* was tested on the beamline FL24 with a Hartmann wavefront sensor, and good agreement between our simulations and the measurements was found (Kuhlmann *et al.*, 2019). Both the gratings and the EM are considered to have a perfect surface. For σ_{RMS} = 0 nm, the figure error is equal to zero along all the surface of both KB mirrors. For the other two cases, *i.e.* σ_{RMS} < 0.3 nm and σ_{RMS} < 0.6 nm, the figure error was normalized to 0.3 nm and 0.6 nm, respectively. In all three cases, the figure error of the PM and the two alignment mirrors is σ_{RMS} < 0.3 nm.

The time-delay compensating monochromator based on the *WPG* calculations produces a focus of 3.0 × 2.0 µm (H × V, FWHM) for λ = 13 nm and divergence θ_{div} = 125 µrad (FWHM), as shown in Fig. 5(*a*). Some small defects appear as a consequence of the asymmetries introduced by the PM slope

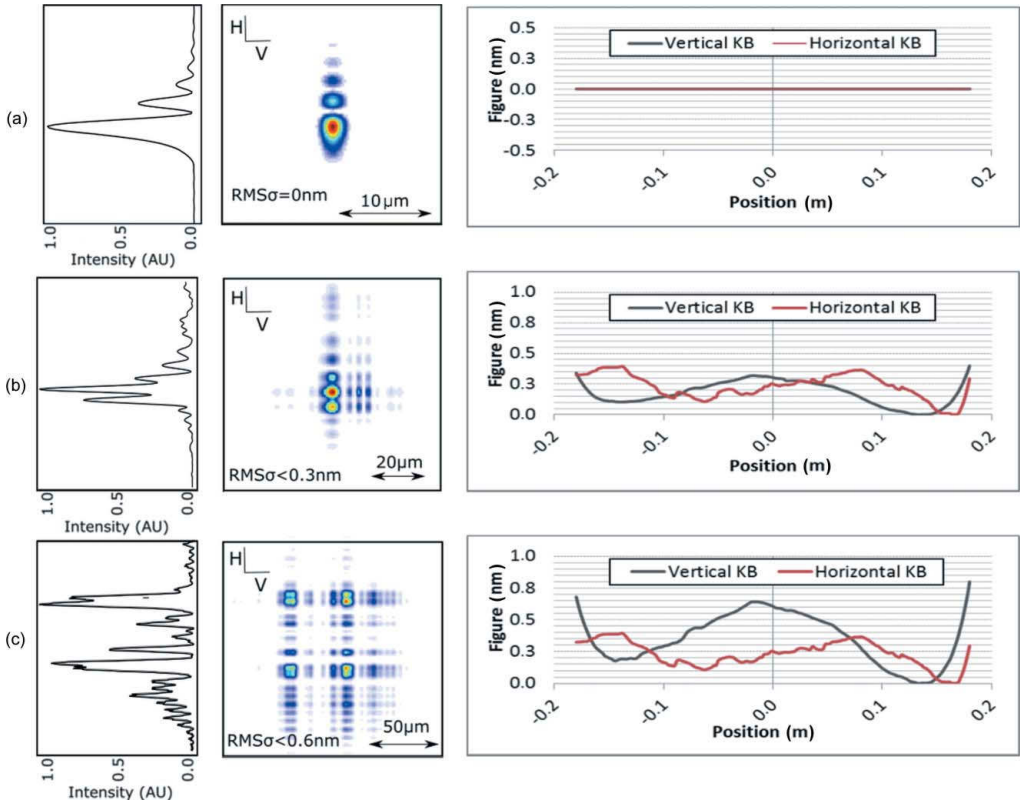

Figure 5
(*a*) Ideal mirror, (*b*) figure errors RMS σ < 0.3 nm and (*c*) figure errors RMS σ < 0.6 nm. The first column shows the horizontal profile of the focus taken at its vertical intensity maximum position, the second column shows the calculated focus and the third column shows the figure error applied in each case in *WPG*.

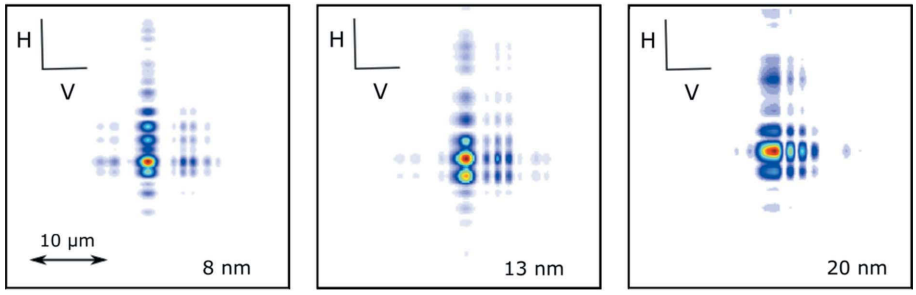

Figure 6
Focus at 2 m of the horizontal KB mirror illuminated at (*a*) 8 nm, (*b*) 13 nm and (*c*) 20 nm, for $\sigma_{RMS} < 0.3$ nm.

error. Geometrically the KB optical system gives demagnification factors of 23 in the horizontal direction and 35 in the vertical direction, providing a geometrical focus comparable to our simulations for a source size of ∼70 µm.

The focus obtained with mirrors degraded by a profile $\sigma_{RMS} < 0.3$ nm shows a decrease of the intensity in the main mode to 21%, while the rest of the energy is scattered into a number of side maxima. When the mirror quality is degraded even more strongly by a profile $\sigma_{RMS} < 0.6$ nm, the effects become more and more pronounced and again a number of additional modes are generated in the focus. For larger wavelengths, although the number of modes is invariant, the distribution of the intensity becomes more and more inhomogeneous as shown in Fig. 6.

5. Conclusions

The *WPG* framework has been upgraded to include the effects of misalignments of optical components within a beamline design. As presented for the time-delay compensating monochromator beamline proposed for FLASH2, wavefront-propagation simulations allow optimization of the beamline transmission and show a much more realistic photon-beam energy distribution at the beamline focus for user experiments. Specifically, three effects were studied: (1) the footprints on the first grating G1, (2) the tolerances for misalignments in the γ, ρ and ζ angles of the EM, and (3) the RMS tolerances for the figure error of the KB mirrors. To obtain realistic results, calculations realized with *GENESIS* for the FLASH2 source and experimental data for divergence and photon spectra were incorporated into the simulations.

Calculations of the footprints at the first grating G1 showed a footprint of 78 mm (FWHM) at 13.5 nm and 110 mm (FWHM) for 20 nm. Based on these results we decided to use a 200 mm length grating to cover at least 4σ of the beam for longer wavelengths.

The wavefront simulations also aimed at determining the tolerances for the alignment of the optical components, which thus have to be taken into account for the mirror-mount motions in the design process. As an example, ρ and ζ angles could be shown to be uncritical in the milliradian range for the movements of the EM; however, the movements of the γ angle needs to be controllable at the microradian scale, *i.e.* steps of 50 µrad or better. The concept for the movement of the mirror chambers at FLASH, which is based on moving the entire mirror chamber outside the vacuum, typically provides the required precision.

Regarding the figure error, RMS values of <0.3 nm are the errors available from mirror manufacturers. However, even this quality of the mirrors figure error shows some degradation of the density distribution and side maxima in the focus of our optical system, which may be relevant for some user experiments.

References

Ackermann, W., Asova, G., Ayvazyan, V., Azima, A., Baboi, N., Bähr, J., Balandin, V., Beutner, B., Brandt, A., Bolzmann, A. *et al.* (2007). *Nat. Photon.* **1**, 336.

Faatz, B., Plönjes, E., Ackermann, S., Agababyan, A., Asgekar, V., Ayvazyan, V., Baark, S., Baboi, N., Balandin, V., Bargen, N., Bican, Y., Bilani, O., Bödewadt, J., Böhnert, M., Böspflug, R., Bonfigt, S., Bolz, H., Borges, F., Borkenhagen, O., Brachmanski, M., Braune, M., Brinkmann, A., Brovko, O., Bruns, T., Castro, P., Chen, J., Czwalinna, M. K., Damker, H., Decking, W., Degenhardt, M., Delfs, A., Delfs, T., Deng, H., Dressel, M., Duhme, H., Düsterer, S., Eckoldt, H., Eislage, A., Felber, M., Feldhaus, J., Gessler, P., Gibau, M., Golubeva, N., Golz, T., Gonschior, J., Grebentsov, A., Grecki, M., Grün, C., Grunewald, S., Hacker, K., Hänisch, L., Hage, A., Hans, T., Hass, E., Hauberg, A., Hensler, O., Hesse, M., Heuck, K., Hidvegi, A., Holz, M., Honkavaara, K., Höppner, H., Ignatenko, A., Jäger, J., Jastrow, U., Kammering, R., Karstensen, S., Kaukher, A., Kay, H., Keil, B., Klose, K., Kocharyan, V., Köpke, M., Körfer, M., Kook, W., Krause, B., Krebs, O., Kreis, S., Krivan, F., Kuhlmann, J., Kuhlmann, M., Kube, G., Laarmann, T., Lechner, C., Lederer, S., Leuschner, A., Liebertz, D., Liebing, J., Liedtke, A., Lilje, L., Limberg, T., Lipka, D., Liu, B., Lorbeer, B., Ludwig, K., Mahn, H., Marinkovic, G., Martens, C., Marutzky, F., Maslocv, M., Meissner, D., Mildner, N., Miltchev, V., Molnar, S., Mross, D., Müller, F., Neumann, R., Neumann, P., Nölle, D., Obier, F., Pelzer, M., Peters, H., Petersen, K., Petrosyan, A., Petrosyan, G., Petrosyan, L., Petrosyan, V., Petrov, A., Pfeiffer, S., Piotrowski, A., Pisarov, Z., Plath, T., Pototzki, P., Prandolini, M. J., Prenting, J., Priebe, G., Racky, B., Ramm, T., Rehlich, K., Riedel, R., Roggli, M., Röhling, M., Rönsch-Schulenburg, J., Rossbach, J., Rybnikov, V., Schäfer, J., Schaffran, J., Schlarb, H., Schlesselmann, G., Schlösser, M., Schmid, P., Schmidt, C., Schmidt-Föhre, F., Schmitz, M., Schneidmiller, E., Schöps, A., Scholz, M., Schreiber, S., Schütt, K., Schütz, U., Schulte-Schrepping, H., Schulz, M., Shabunov, A., Smirnov, P., Sombrowski, E., Sorokin, A., Sparr, B., Spengler, J., Staack, M., Stadler, M., Stechmann, C., Steffen, B., Stojanovic, N., Sychev, V., Syresin, E., Tanikawa, T., Tavella, F., Tesch, N., Tiedtke, K., Tischer, M., Treusch, R., Tripathi, S., Vagin, P., Vetrov, P., Vilcins, S., Vogt, M.,

Wagner, A. Z., Wamsat, T., Weddig, H., Weichert, G., Weigelt, H., Wentowski, N., Wiebers, C., Wilksen, T., Willner, A., Wittenburg, K., Wohlenberg, T., Wortmann, J., Wurth, W., Yurkov, M., Zagorodnov, I. & Zemella, J. (2016). *New J. Phys.* **18**, 062002.
Flöter, B., Juranić, P., Kapitzki, S., Keitel, B., Mann, K., Plönjes, E., Schäfer, B. & Tiedtke, K. (2010). *New J. Phys.* **12**, 083015.
Frassetto, F., Ploenjes, E., Kuhlmann, M. & Poletto, L. (2014). *Proc. SPIE*, **9210**, 92100I.
Gerasimova, N., Dziarzhytski, S. & Feldhaus, J. (2011). *J. Mod. Opt.* **58**, 1480–1485.
Huang, Z., *et al.* (2013). *Brightness and coherence of synchrotron radiation and FELs.* Technical Report. SLAC National Accelerator Laboratory, Menlo Park, CA 94025, USA.
Kuhlmann, M., Keitel, B., Plönjes, E., Ruiz-Lopez, M., Rönsch-Schulenburg, J. & Zangrando, M. (2019). *J. Synchrotron Rad.* **26**. To be published.
Martins, M., Wellhöfer, M., Hoeft, J., Wurth, W., Feldhaus, J. & Follath, R. (2006). *Rev. Sci. Instrum.* **77**, 115108.
Poletto, L., Frassetto, F., Brenner, G., Kuhlmann, M. & Plönjes, E. (2018). *J. Synchrotron Rad.* **25**, 131–137.
Poletto, L., Villoresi, P., Frassetto, F., Calegari, F., Ferrari, F., Lucchini, M., Sansone, G. & Nisoli, M. (2009). *Rev. Sci. Instrum.* **80**, 123109.
Raimondi, L., Svetina, C., Mahne, N., Cocco, D., Capotondi, F., Pedersoli, E., Manfredda, M., Kiskinova, M., Keitel, B., Brenner, G., Plönjes, E, Mey, T., Mann, K. & Zangrando, M. (2014). *Proc. SPIE*, **9208**, 920804.
Rakitin, M. S., Chubar, O., Moeller, P., Nagler, R. & Bruhwiler, D. L. (2017). *Proc. SPIE*, **10388**, 103880R.
Rebuffi, L. & Sánchez del Río, M. (2016). *J. Synchrotron Rad.* **23**, 1357–1367.
Reiche, S. (1999). *Nucl. Instrum. Methods Phys. Res. A*, **429**, 243–248.
Samoylova, L., Buzmakov, A., Chubar, O. & Sinn, H. (2016). *J. Appl. Cryst.* **49**, 1347–1355.
Sanchez del Rio, M., Bianchi, D., Cocco, D., Glass, M., Idir, M., Metz, J., Raimondi, L., Rebuffi, L., Reininger, R., Shi, X., Siewert, F., Spielmann-Jaeggi, S., Takacs, P., Tomasset, M., Tonnessen, T., Vivo, A. & Yashchuk, V. (2016). *J. Synchrotron Rad.* **23**, 665–678.
Tanikawa, T., Hage, A., Kuhlmann, M., Gonschior, J., Grunewald, S., Plönjes, E., Düsterer, S., Brenner, G., Dziarzhytski, S., Braune, M., Brachmanski, M., Yin, Z., Siewert, F., Dzelzainis, T., Dromey, B., Prandolini, M. J., Tavella, F., Zepf, M. & Faatz, B. (2016). *Nucl. Instrum. Methods Phys. Res. A*, **830**, 170–175.
Tiedtke, K., Braune, M., Brenner, G., Dziarzhytski, S., Faatz, B., Feldhaus, J., Keitel, B., Kuhlmann, M., Kühn, H., Plönjes, E., Sorokin, A. A. & Treusch, R. (2013). *Proceedings of the 35th Free-Electron Laser Conference (FEL2013)*, 26–30 August 2013, New York, NY, USA, pp. 417–420. TUPSO81.